Cellulose (2025) 32:3633–3649
https://doi.org/10.1007/s10570-025-06464-4

ORIGINAL RESEARCH

Synthesis of Ni-W catalysts supported on fruit peel waste-derived carbons for the efficient ethylene glycol production from cellulose

Lucília S. Ribeiro · Rafael G. Morais · Alexandre C. Damas · José J. M. Órfão · M. Fernando R. Pereira

Received: 6 November 2024 / Accepted: 25 February 2025 / Published online: 22 March 2025

Abstract Fruit peel waste-derived carbons synthesized from orange and banana peels by hydrothermal carbonization were employed as supports in the preparation of nickel-tungsten heterogeneous catalysts. These bimetallic catalysts were fully characterized by several techniques and evaluated for the direct conversion of cellulose into ethylene glycol (EG) in aqueous medium. The catalysts showed noteworthy activity in cellulose conversion (100%), resulting in an impressive EG yield of up to 50% over the glucose-derived carbon supported Ni-W catalyst. Furthermore, notable EG yields of around 35 and 45% were reached over orange and banana peel-derived carbon supported catalysts, respectively. The best performing catalyst was further tested in four reusability experiments, displaying excellent stability. The results obtained here are amongst the best ever reported for the one-pot cellulose conversion to EG over carbon-supported catalysts. These findings suggest that fruit peel, namely banana peel, holds great potential as a catalytic support, thus presenting a viable alternative for waste valorization in lignocellulosic biorefining.

Keywords Cellulose conversion · Fruit wastes valorization · One-pot process · Heterogeneous catalysis · Ethylene glycol

Abbreviations

AAS	Atomic absorption spectroscopy
AC	Activated carbon
BC	Biochar
BET	Brunauer–Emmett–Teller
BMC	Ball-milled cellulose
BSED	Backscattered electron detector

Lucília S. Ribeiro and Rafael G. Morais have contributed equally to this work.

Supplementary Information The online version contains supplementary material available at https://doi.org/10.1007/s10570-025-06464-4.

L. S. Ribeiro (✉) · R. G. Morais · A. C. Damas · J. J. M. Órfão · M. F. R. Pereira
LSRE-LCM – Laboratory of Separation and Reaction Engineering - Laboratory of Catalysis and Materials, Faculty of Engineering, University of Porto, Rua Dr. Roberto Frias, 4200-465 Porto, Portugal
e-mail: lucilia@fe.up.pt

R. G. Morais
e-mail: rgm@fe.up.pt

A. C. Damas
e-mail: up202208666@edu.fe.up.pt

J. J. M. Órfão
e-mail: jjmo@fe.up.pt

M. F. R. Pereira
e-mail: fpereira@fe.up.pt

L. S. Ribeiro · R. G. Morais · A. C. Damas · J. J. M. Órfão · M. F. R. Pereira
ALiCE – Associate Laboratory in Chemical Engineering, Faculty of Engineering, University of Porto, Rua Dr. Roberto Frias, 4200-465 Porto, Portugal
e-mail: rgm@fe.up.pte-mail: up202208666@edu.fe.up.pte-mail: jjmo@fe.up.pte-mail: fpereira@fe.up.pt

CB	Carbonized banana
CG	Carbonized glucose
CNF	Carbon nanofibers
CNT	Carbon nanotubes
CO	Carbonized orange
DHA	Dihydroxyacetone
EDS	Energy dispersive spectroscopy
EG	Ethylene glycol
ETD	Everhart–Thornley detector
FA	Formic acid
ERY	Erythritol
GLY	Glycerol
HA	Hydroxyacetone
HPLC	High performance liquid chromatography
HTC	Hydrothermal carbonization
ICP-OES	Inductively coupled plasma-optical emission spectrometry
MCC	Microcrystalline cellulose
NC	N-doped carbon
PG	Propylene glycol (1,2-propanediol)
RAC	Retro-aldol condensation
SEM	Scanning electron microscopy
SOR	Sorbitol
TEM	Transmission electron microscopy
TGA	Thermogravimetric analyses
THR	Threitol
TOC	Total organic carbon
XPS	X-ray photoelectron spectroscopy
XRD	X-ray diffraction

Introduction

Ethylene glycol (EG) is a valuable chemical mainly used for antifreeze formulations and as a monomer in the manufacture of polyester fibres such as polyethylene terephthalate (Li et al. 2024). It is currently obtained from non-renewable petroleum and coal resources through the production of harmful intermediate compounds (Goc et al. 2023; Gao et al. 2023). Consequently, looking toward a more sustainable process, a possible route from the catalytic transformation of renewable resources like biomass, particularly polycarbohydrates such as cellulose, has been pointed out in recent years (Wang and Zhang 2013; Wang et al. 2023; Li et al. 2015). This process involves three subsequent steps: hydrolysis of cellulose to glucose, followed by glucose's retro-aldol condensation (RAC) into glycolaldehyde and subsequent hydrogenation to EG (Wang and Zhang 2013; Ribeiro et al. 2018b).

So far, the reported yields of EG from cellulose range up to 76.1%, which was obtained over a SBA-15 supported Ni–W bimetallic catalyst (Zheng et al. 2010). However, this catalyst could not be reused due to the complete collapse of the mesoporous structure of SBA-15, which is a limitation of commercially available metal oxide supports such as silica and alumina in subcritical water. Accordingly, carbon supports are preferred due to their high hydrothermal stability and high resistance to acid and base attack (Ribeiro et al. 2024). Furthermore, the catalytic support has a great influence since it regulates not only the structure of active components, but also the catalyst's stability. Thus, developing highly active, selective and stable carbon-supported catalysts with multifunctional active catalytic sites for hydrolysis, RAC and hydrogenation is of great importance.

On the other hand, to help tackle the current huge accumulation of wastes, the synthesis of carbon materials from different waste materials is becoming an area of extensive research. In fact, the utilization of biomass-derived carbons over commercially available expensive carbon materials (e.g., carbon nanotubes) has been subject of great focus in the past few years due to its advantages such as low cost, high quality, easy availability and also environmental suitability (Ziegler et al. 2017; Ribeiro et al. 2019). Besides, biomass-derived carbons have excellent properties like high surface area, high porosity degree and abundance of surface functionalities, thus making them promising materials to be used as supports for the synthesis of catalysts (Liu et al. 2015; Kempasiddaiah et al. 2021). Although many works have reported the development of waste-derived carbons for diverse applications (Kempasiddaiah et al. 2021; Shetty et al. 2023; Yadav and Ahmaruzzaman 2022; Teng et al. 2023; Miah et al. 2023; Zhu et al. 2023; Inkoua et al. 2023; Ma et al. 2021; Tran et al. 2022; Satira et al. 2021), as far as we are concerned, only one work has reported the synthesis of catalysts supported on carbon derived from food waste (i.e., pomelo peel) for cellulose conversion to EG (Huang et al. 2022). However, due to metal leaching and catalyst loss, the EG yield decreased significantly after the first recycling test.

In this study, exploring our research group's extensive experience in lignocellulosic biomass catalytic

conversion, carbon materials and catalysts synthesis, we aimed to recycle and valorize food waste (i.e., orange and banana peels) for the synthesis of renewable waste-derived carbon supported catalysts to produce EG directly from cellulose, to address one of the most reported drawbacks in the literature: the lack of catalytic stability. Currently, the five most produced fruits in the world are bananas (135,112,300 t), watermelons (99,957,600 t), apples (95,835,965 t), oranges (76,410,040 t) and grapes (74,942,570 t), while the most produced fruits in Portugal are grapes (903,510 t), oranges (378,450 t), apples (291,190 t), pears (132,28 t) and bananas (28,460 t) (Worldostats 2024). Among these fruits, the peels of grapes, apples and pears are edible. Thus, banana and orange peels were selected for this work since these are two of the most consumed fruits in Portugal (leading to a higher amount of waste) and their peels are inedible, thereby not competing with food.

Experimental

Chemicals

Unless stated otherwise, all the chemicals were used directly without purification. Microcrystalline cellulose (MCC) (5.1% loss on drying, 0.35 g cm^{-3} bulk density, 0.025% residue on ignition, degree of polymerization of 221, 6.3 nm of diameter) was acquired from Alfa Aesar, while banana and orange peels were collected from kitchen waste. Nickel(II) nitrate hexahydrate ($Ni(NO_3)_2{\cdot}6H_2O, \geq 99\%$) and ammonium metatungstate hydrate ($(NH_4)_6W_{12}O_{39}{\cdot}xH_2O$, 99.99%) were provided by Merck and Thermo Scientific, respectively. Ultrapure water (18.2 µS cm^{-1} conductivity), obtained in a Milli-Q Millipore System, was used for the preparation of all the solutions. Nitrogen (N_2, 99.999%) and hydrogen (H_2, 99.99999%) were supplied by Air Liquide.

Synthesis of materials

The substrate (microcrystalline cellulose) was ball-milled prior to the reaction for 4 h at 20 s^{-1} in a Retsch Mixer Mill MM200, as described in detail elsewhere (Ribeiro et al. 2015).

Fruit peel-derived carbons were synthesized by hydrothermal carbonization (HTC) of banana and orange peels, followed by a thermal treatment to develop the resulting materials' porosity (Ribeiro et al. 2024). Initially, the fruit peels were dried naturally and, then, cut into small pieces of approximately 0.5–1.0 cm. Afterwards, the fruit peels (15 wt %) and ultrapure water (85 wt %) were mixed and sonicated before being enclosed in a Teflon-lined autoclave (stainless steel). This mixture was then heated to 180 ºC and maintained for 12 h, resulting in a brown material that was dried at 100 ºC overnight after being thoroughly washed with ultrapure water. Afterwards, the dried material was treated under inert (N_2) atmosphere for 2 h at 700 °C under a 100 cm^3 min^{-1} flow rate. The resulting samples were denoted as carbonized banana (CB) and carbonized orange (CO). Moreover, a carbon support was prepared by hydrothermal polymerization of glucose followed by thermal treatment using the same conditions abovementioned, resulting in sample CG.

Ni-W bifunctional catalysts were synthesized using the aforementioned materials. In this instance, two precursors (nickel(II) nitrate hexahydrate and ammonium metatungstate hydrate) were employed and introduced in a gradual manner to the supports via incipient wetness co-impregnation, with the objective of preparing catalysts exhibiting a nominal metal loading of 20 wt % Ni and 10 wt % W. The selection of these metal contents was based on a previous study (Ribeiro et al. 2024). Subsequently, the materials were dried overnight and then treated for 3 h at 500 °C using a nitrogen atmosphere, followed by 3 h of reduction under a hydrogen atmosphere at the same temperature and a flow rate of 100 cm^3 min^{-1}. A fixed heating ramp of 10 °C min^{-1} was used to carry out all thermal treatments. The samples were named according to the carbon support used, resulting in samples Ni-W/CG, Ni-W/CO and Ni-W/CB.

Characterization techniques

The textural properties of the materials were analysed by N_2 adsorption–desorption isotherms at – 196 ºC in a Quantachrome NOVA 4200e Surface Area and Pore Size analyser, after degassing at 150 ºC for 3 h under vacuum. Total specific surface area (S_{BET}) was estimated according to the Brunauer–Emmett–Teller (BET) method, the micropore volume ($V_{\mu pores}$) and external surface area (S_{ext}) were determined by the *t*-method, and the total pore volume (V_p) was

calculated based on the amount of N_2 adsorbed at the saturation point ($P/P_0 = 0.99$).

Thermogravimetric analyses (TGA) of all the materials were performed in duplicate in a STA 409 PC/4/H Luxx Netzsch apparatus, using a heating rate of 10 ºC min^{-1} from 50 to 900 ºC under N_2. Then, an isotherm at 900 ºC under the same atmosphere was kept for 7 min, followed by another isotherm at 900 ºC under air for another 13 min. Then, the ash content was estimated as the residue after this final oxidation.

Atomic absorption spectroscopy (AAS) was carried out using a Unicam Solar 939 equipment to quantify the nickel loading of the synthesized catalysts. Prior to the analysis, the catalysts were digested in a solution of nitric acid for 15 min at 180 ºC.

The surface composition of the prepared catalysts was studied by X-ray photoelectron spectroscopy (XPS) in a Kratos AXIS Ultra HAS spectrometer. The operation conditions were 15 kV (90 W) using a fixed analyzer transmission mode and a monochromatic Al Kα radiation (1486.7 eV).

Raman spectroscopy was employed to investigate the defects and strain of the prepared materials using an Alpha 300 apparatus coupled with a 532 nm monochromatic wavelength laser.

The catalysts' morphology and distribution of the elements of interest were studied by scanning electron microscopy (SEM), energy dispersive spectroscopy (EDS) and elemental mapping using a FEI Quanta 400 FEG ESEM/EDAX Genesis X4M equipment. Moreover, the SEM analyses were achieved using an Everhart–Thornley detector (ETD) and a backscattered electron detector (BSED), while EDS and elemental mapping measurements were obtained with a Si(Li) detector. Further studies were conducted by transmission electron microscopy (TEM) using a high-resolution scanning/transmission electron microscope FEI Talos F200X operating at 200 kV.

The crystalline phases' composition was analyzed by X-ray diffraction (XRD) using a 1.541874 Å wavelength Cu Kα radiation on a X'Pert Pro diffractometer (PANalytical, Malvern, UK) at 40 mA and 45 kV composed by a PIXcel detector.

Catalysts' evaluation and products analysis

Ball-milled cellulose (750 mg) and catalyst (300 mg) were mixed with deionized water (300 mL) in a 1000 mL Parr Instruments high-pressure reactor (USA Mod. 5120). Subsequently, the reactor was closed and purged three times with N_2. Then, the system was heated up to 205 ºC under stirring at 300 rpm. As soon as the desired temperature was attained, the reaction was started by changing to 5 MPa of H_2 and carried out for 5 h. During the reaction, samples were periodically withdrawn, centrifuged at 13,500 rpm for 5 min in a VWR Microstar12 apparatus and filtered for subsequent analysis. At the end of the reaction, the catalyst was recovered from the reaction mixture by filtration, washed with deionized water and dried in an oven at 100 ºC for 24 h. The collected reaction mixture was analysed by inductively coupled plasma-optical emission spectrometry (ICP-OES), using a Thermo Fisher Scientific iCAP 7000 spectrometer, to test for metal leaching. Reusability tests were performed for four successive runs, which required adding a small amount of fresh catalyst (< 5 wt %) before each test to maintain the desired 300 mg of catalyst, due to small mass losses during the recovering process; it should be noted that no extra reduction/treatment of the catalyst was conducted. Furthermore, reproducibility tests were carried out in triplicate, and the results showed a standard deviation of less than 6 and 1.8% for conversion and yield, respectively.

The water-soluble products were identified and quantified by high performance liquid chromatography (HPLC). The analysis was carried out using an Elite LaChrom HITACHI equipment, in which the products' separation was achieved by an Alltech OA-1000 ion exclusion column (300 × 6.5 mm) using a refractive index detector. A solution of 5 mM of H_2SO_4 was used as mobile phase at a flow rate of 0.5 mL min^{-1}. Then, the products' yields were determined as the ratio between the number of moles of carbon in each product (measured by HPLC) and the number of moles of carbon in the initial cellulose. Additionally, total organic carbon (TOC) analyses were performed in a TOC-L Shimadzu apparatus. The cellulose conversion (X) was estimated as the ratio between the number of moles of TOC in the resultant liquid and the number of moles of carbon in the initial cellulose.

Results and discussion

Materials' characterization

Microcrystalline and ball-milled cellulose are characterized elsewhere (Ribeiro et al. 2015), as well as the fruit peels (Ribeiro et al. 2024).

The textural properties of the fruit peels, the synthesized carbon supports and respective bimetallic catalysts were determined using the N_2 adsorption–desorption isotherms, as illustrated in Fig. S1. The calculated parameters are presented in Table 1. The fruit peels exhibit a negligible specific surface area (S_{BET}), external area (S_{ext}) and no microporosity ($V_{\mu pores}$). Following the thermal treatments employed to develop both the fruit-peel derived carbon supports and the glucose sample, all carbon supports exhibited higher S_{BET} and expanded microporosity. Nevertheless, differences are observed among the three supports. The banana-derived carbon (CB) displayed the highest S_{BET} of the carbon supports (489 $m^2\ g^{-1}$) followed by CG (427 $m^2\ g^{-1}$) and CO (334 $m^2\ g^{-1}$). In fact, when comparing the two waste-derived carbons with the glucose-derived carbon (CG), the S_{BET} obtained over CB is closer to that of CG, which could be attributed to the fact that banana peel has a higher content of water-soluble sugars like saccharose, glucose and fructose (47.5%) than orange peel (38.2%) (Ribeiro et al. 2024). Furthermore, CB presented a markedly higher S_{ext} (111 $m^2\ g^{-1}$) in comparison to CG and CO (31 and 38 $m^2\ g^{-1}$, respectively), while CG developed the highest degree of microporosity. With regard to the bimetallic catalysts, a reduction in S_{BET} was observed in comparison to the carbon support, albeit to varying degrees (Ni-W/CG – 9%, Ni-W/CO – 3% and Ni-W/CB – 27%) and a slight loss of $V_{\mu pores}$. This variation is likely attributable to the incorporation of metal within the porous structure and the contribution of the metallic particles' surface area, which represents a substantial proportion of the catalysts' mass. Regarding the S_{ext}, it is noteworthy that Ni-W/CB displayed a notable loss compared to CB. Lastly, a slight increase in V_p was observed in samples Ni-W/CG and Ni-W/CO and decreased in Ni-W/CB. Following the reusability runs, the Ni-W/CB catalyst exhibited a loss of S_{BET}, $V_{\mu pores}$ and V_p compared to the fresh catalyst. However, there was an increase in its S_{ext} from 42 to 77 $m^2\ g^{-1}$. Those decreases may be attributed to a shift of the metal species closer to the catalyst's surface, as observed by XPS (as shown later), which can be partially blocking the pores and hindering the passage of N_2 to the innermost pores during adsorption analysis. However, their aggregation on the outer surfaces of the carbon support, as observed by XRD (as presented later), increases the accessible external area for reactions, even if the internal surface area and pore volume are reduced.

Thermogravimetric analyses (TGA) were performed on the fruit peels, carbon supports and the fresh bimetallic catalysts derived from the fruit peels. The ash content obtained is displayed in Table 1. The TGA results obtained for the fruit peels demonstrated that both had ashes in their content, with the banana

Table 1 Characterization of materials

Material	S_{BET} ($m^2\ g^{-1}$)	S_{ext} ($m^2\ g^{-1}$)	$V_{\mu pores}$ ($cm^3\ g^{-1}$)	V_p ($cm^3\ g^{-1}$)	Ashes (wt %)	Ni (wt %)	Ni crystallite size (nm)
Orange peel	3.6	3.6	0.000	0.03	3	–	–
Banana peel	4.1	4.1	0.000	0.02	9	–	–
CG	427	31	0.165	0.20	0	–	–
CO	334	38	0.120	0.24	5	–	–
CB	489	111	0.139	0.41	9	–	–
Ni-W/CG	388	37	0.147	0.21	–	23.0	16.9
Ni-W/CO	325	38	0.119	0.28	–	22.2	21.8
Ni-W/CB	358	42	0.133	0.36	–	21.8	21.3
Ni-W/CB [a]	239	77	0.066	0.25	–	–	29.4

[a] After four reusability tests

peel presenting thrice the value of the orange peel (9% *vs*. 3%, respectively). The ashes on the fruit peels were expected due to their varied elemental composition that contains several types of metals (Orozco et al. 2014; Lam et al. 2018). In fact, EDS analysis (Fig. S3) confirmed the presence of Ca for Ni-W/CO and Ni-W/CB. Despite that, Ca is not an active site for this reaction, so the presence of ashes (9% for Ni-W/CB) did not affect the catalyst performance, as later observed. Regarding the carbon supports, the CG sample did not present any ashes, which is due to the very high purity of the glucose employed and the lack of any metallic compounds added to its synthesis. As for the CO sample, the ash content slightly increased, which can be attributed to some carbon burn-off during the carbonization, which led to a higher relative presence of metal compounds. Lastly, the CB support did not exhibit any change to its ash content after carbonization.

The quantification of the presence of Ni on the catalysts was investigated by atomic absorption spectroscopy (AAS) and the results are presented in Table 1. All fresh catalysts showed a Ni content slightly above the theoretical value (20 wt %), probably due to some burn-off of the carbon support.

Figure 1 and Fig. 2 exhibit deconvoluted Ni and W spectra, respectively, while Table 2 shows the surface composition, as determined by XPS. The XPS analysis showed that the surface atomic percentages of Ni and W in the fresh catalysts are very similar (0.8:0.6, 2.1:1.8 and 1.1:1.1 Ni at %:W at %, for Ni-W/CG, Ni-W/CO and Ni-W/CB, respectively), with a slightly higher contribution from Ni. This is in contrast to theoretical calculations, as a 2:1 mass ratio of Ni:W would result in a 0.76:1 Ni:W atomic ratio. This may indicate that Ni favours a more superficial incorporation on the supports than its W counterpart. After the reusability runs, the Ni-W/CB catalysts showed about 1/3 of their initial W surface content, while the Ni content increased to more than 5 times (5.8 at %). The XPS results seem to indicate that Ni has preferentially migrated to the surface of the catalyst after use. With regard to W, if it followed the same trend as Ni and half of its content was removed from the catalyst, the at % obtained is similar to the expected one. The deconvolution of the Ni 2p region revealed two peaks, one corresponding to Ni^0 at 852.8 ± 0.1 eV (Moulder and Chastain 1992) and one corresponding to Ni^{2+} at 856.3 ± 0.3 eV (Moulder and Chastain 1992). In addition, a satellite peak is observed at higher eV. It was observed that both species were well represented in the spectra, so their ratios (Ni^{2+}/Ni^0) were analysed. Ni-W/CB showed the highest Ni^{2+}/Ni^0 ratio (1.79) in comparison to Ni-W/CO and Ni-W/CG (1.66 and 1.35, respectively). After the reusability runs, practically no Ni^0 was detected, which could indicate that it had been oxidized, especially considering that the Ni content on the catalyst surface was 5 times that of the fresh catalyst. Regarding the deconvolution of the W 4f spectra, two different species were observed: i) W^0 at 31.8 ± 0.1 eV and its doublet at 33.7 ± 0.2 eV (Moulder and Chastain 1992) and ii) W^{6+} at 35.7 ± 0.2 eV and its doublet at 37.8 ± 0.2 eV (Ganbavle et al. 2014). In this case, Ni-W/CB has the highest amount of W in its oxidized form followed by Ni-W/CO and Ni-W/CG. After the reusability reactions, no metallic W was detected on the catalyst's surface, similarly to what was observed for Ni.

The variation of the defects' degrees upon incorporating the metallic elements and after recycling the most promising catalyst was studied by Raman spectroscopy. The spectra obtained for carbon supports and the bimetallic catalysts are displayed in Fig. 3. Regardless of the presence of metallic elements, all spectra exhibited four main peaks: i) a D* band (ca. 1170 cm^{-1}) characteristic of disorder-induced modes in carbon, ii) the D band (ca. 1350 cm^{-1}) correlated with the defects on the carbon structure, iii) D' band (ca. 1500 cm^{-1}) associated with amorphous structures in the material and functional groups, and iv) the G band (ca. 1580 cm^{-1}) associated to the graphitic nature of the sample (Yadav et al. 2020). Regarding the carbon supports, both carbonized fruit peels displayed a very similar A_D/A_G ratio (0.79) and a higher graphitic nature than the CG support (0.87). The incorporation of Ni and W brought closer the structural crystallinity of the fruit-derived catalysts compared to CG. The A_D/A_G ratio was increased for the banana and orange-derived bimetallic catalysts (0.81 and 0.85, respectively) and decreased for the glucose-derived carbon (0.85). After the reusability runs, the A_D/A_G ratio of Ni-W/CB remained very similar (0.80), indicating no significant carbon structural changes. No correlation was observed between this ratio and the performance of the fresh catalyst as Ni-W/CB displayed the lowest A_D/A_G ratio of the three catalysts, but did not show the worst performance, whereas Ni-W/CO exhibited the highest ratio

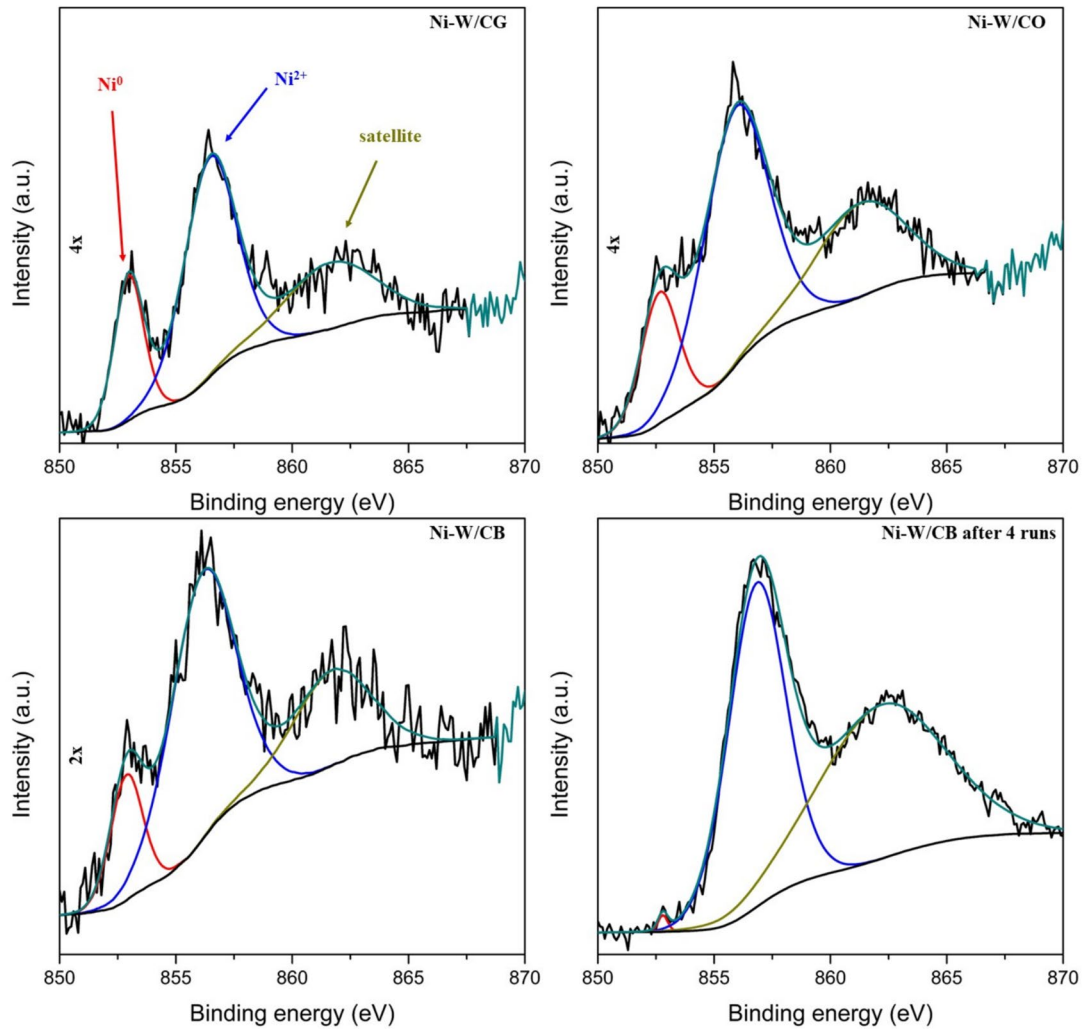

Fig. 1 XPS spectra of Ni for the Ni-W bimetallic catalysts

and the worst performance of the group. Moreover, the reusability tests and Raman spectra of the banana peel-derived catalyst revealed no significant changes, indicating that no correlation between these factors and the catalyst's stability could be stablished.

The morphology of the prepared carbon supports was investigated by SEM and the obtained micrographs are displayed in Fig. 4. The SEM images of the samples synthesized using fruit peels (Fig. 4b and c) showed surfaces with irregular morphology, which may be related to their natural origin and corresponding complex structure. On the other hand, the CG prepared by polymerization of glucose followed by carbonization shows generally spherical structures (Fig. 4a). To further investigate this, the bimetallic catalysts were studied using a BSED and by EDS. The obtained images and EDS results are presented in Fig. S2 and Fig. S3, respectively. All the materials showed a contrast between the areas with the least amount of metals, the darker areas, and those with the greatest presence of these elements, the lighter areas (Fig. S2). Analysis of these zones (Fig. S3) showed that the incorporated metallic elements, Ni and W, are present in both zones, with a slight increase in their presence in the brighter zones. In addition, it is possible to identify other elements, such as Ca, in the catalysts prepared with banana and orange peels that would already be

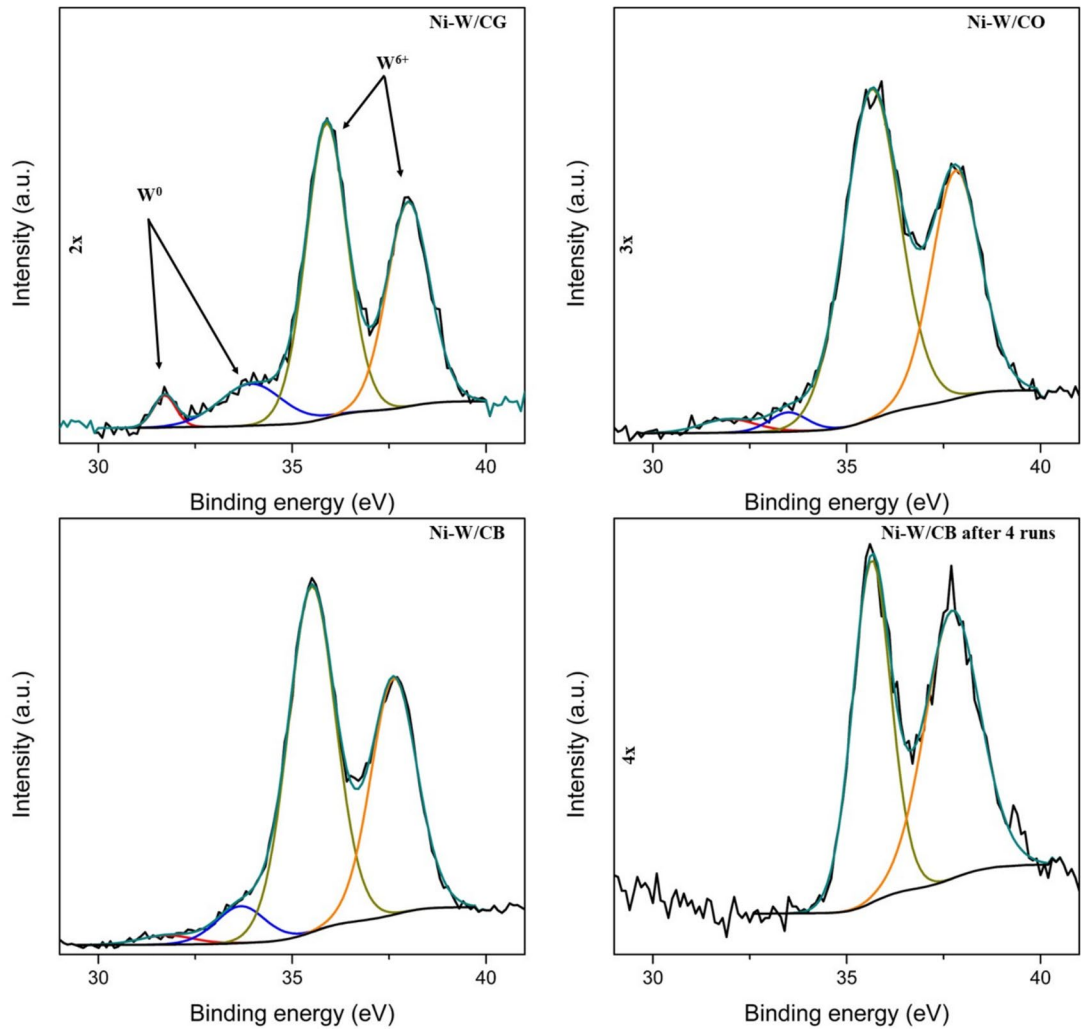

Fig. 2 XPS spectra of W for the Ni-W bimetallic catalysts

Table 2 XPS data obtained for the Ni-W bimetallic catalysts

Catalyst	C (at %)	N (at %)	O (at %)	Ni (at %)	W (at %)	Ni^0 (%)	Ni^{2+} (%)	Ni^{2+}/Ni^0	W^0 (%)	W^{6+} (%)
Ni-W/CG	85.6	0.3	12.7	0.8	0.6	42.5	57.5	1.35	13.7	86.3
Ni-W/CO	81.1	0.9	14.1	2.1	1.8	37.6	62.4	1.66	7.8	92.2
Ni-W/CB	84.2	1.7	11.9	1.1	1.1	35.8	64.2	1.79	4.9	95.1
Ni-W/CB[a]	73.7	0.9	19.2	5.8	0.4	0.8	99.2	124	0.0	100

[a]After four reusability tests

present in these raw materials. Nonetheless, Ni-W/CB after runs' BSED images did not display the same dispersion of the metallic contrast observed by the brighter areas as its fresh counterpart. These micrographs suggest that the metallic species had a higher agglomeration on the catalyst's surface after the reusability runs. Moreover, EDS analyses exhibited a higher contribution of Ni in both darker and

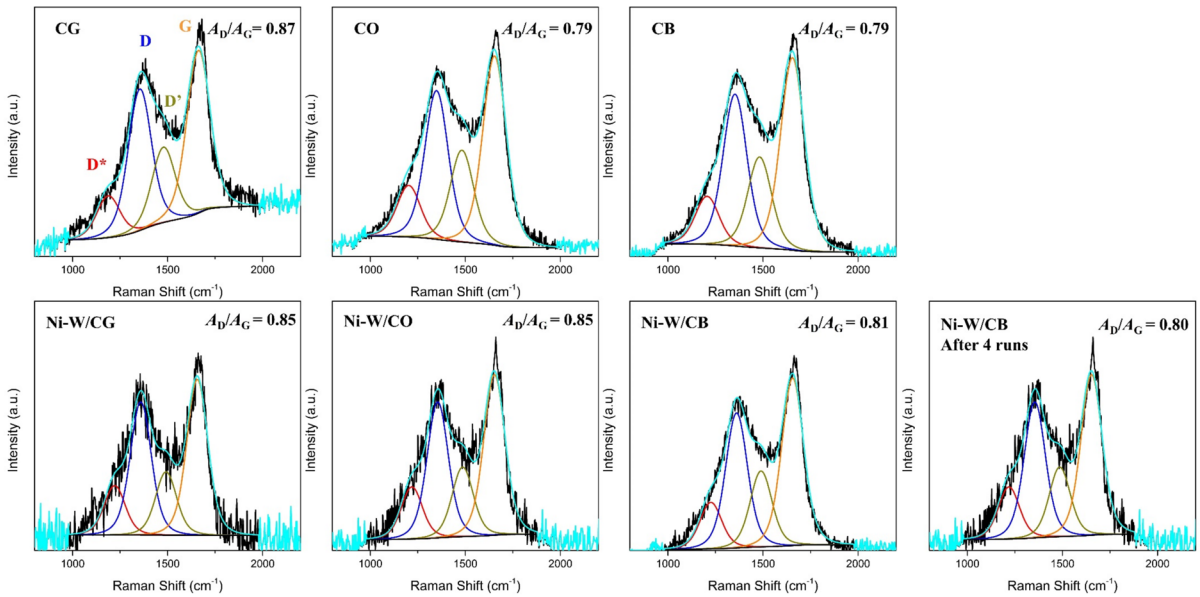

Fig. 3 Raman spectra of the carbon materials and respective Ni-W bimetallic catalysts

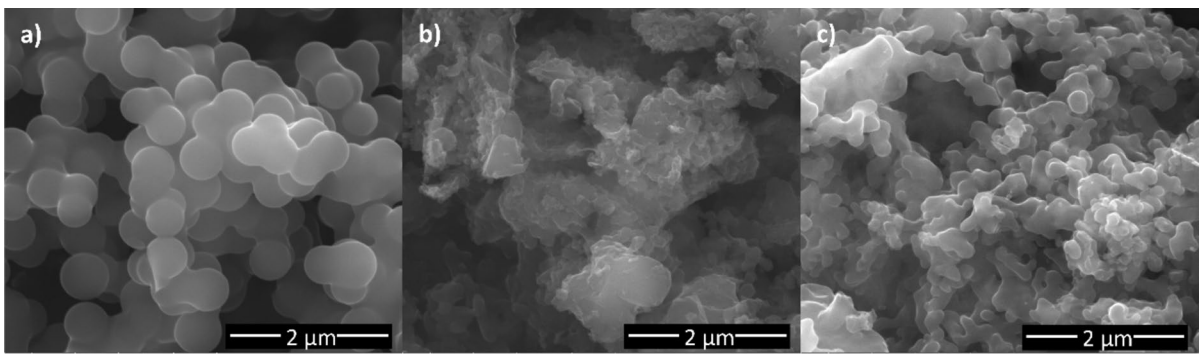

Fig. 4 SEM images of **a** CG, **b** CO and **c** CB

lighter areas for the recycled catalyst than the fresh Ni-W/CB, which suggests that its presence on the surface is superior after the reusability runs. The bimetallic catalysts were then subjected to elemental mapping to further understand the metals' distribution on the carbon supports. This analysis showed a good dispersion of the metallic elements throughout the area of the catalysts analyzed, with some areas showing a greater degree of agglomeration of both Ni and W (Fig. S4).

To further understand the morphology of the samples, the bimetallic catalysts were also analyzed by TEM and the resulting images are displayed in Fig. 5.

All materials show small metallic particles dispersed throughout the carbon support and some zones where agglomeration has taken place. Nonetheless, when analysing the particle size distribution of the metallic phase, it was observed that Ni-W/CB had the smallest average particle size (15 ± 8 nm) of the three fresh catalysts, followed by Ni-W/CG (17 ± 7 nm) and Ni-W/CO (18 ± 7 nm). For the used catalyst Ni-W/CB, it was not possible to determine

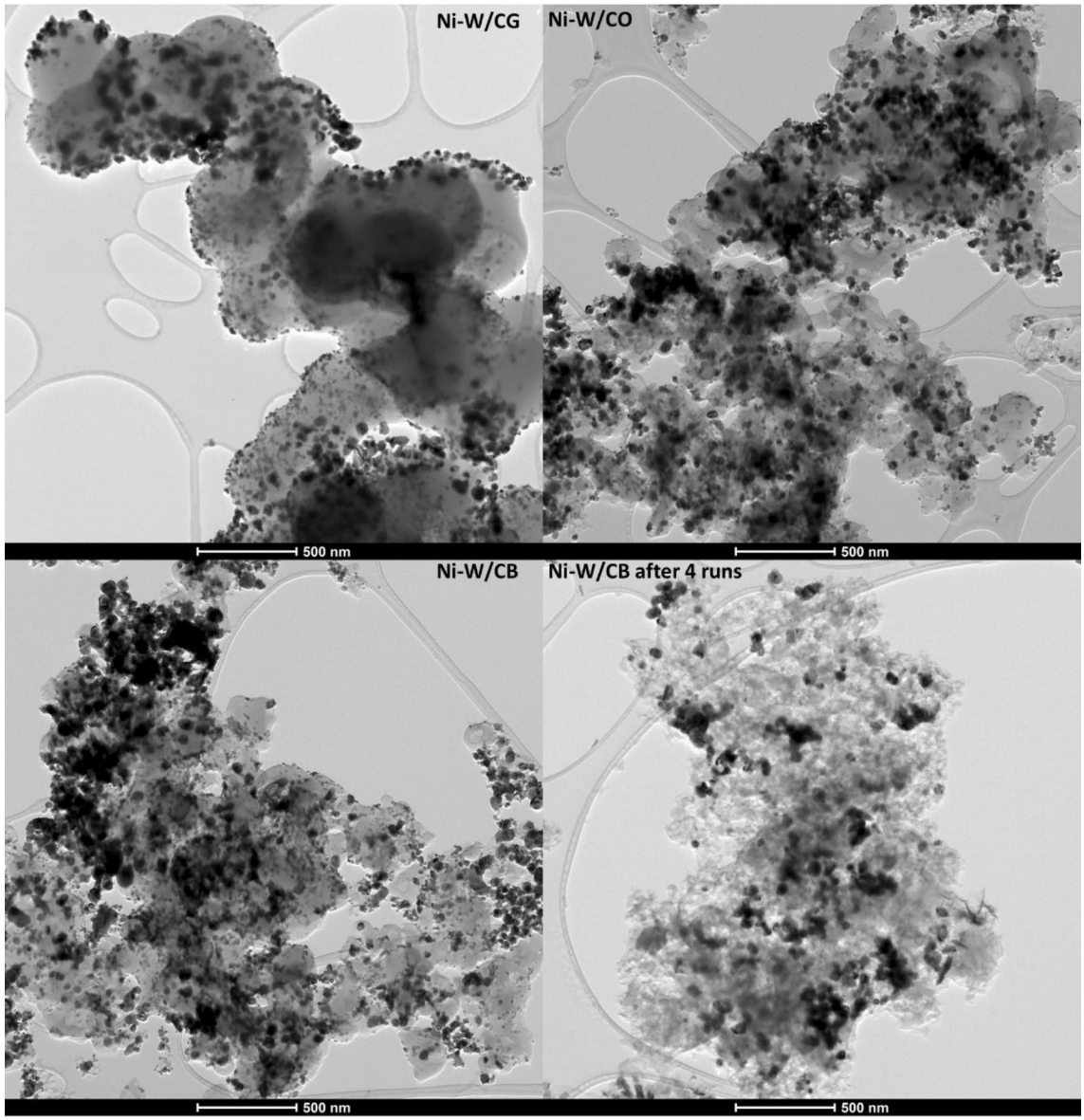

Fig. 5 TEM images of Ni-W/CG, Ni-W/CO, Ni-W/CB and Ni-W/CB after 4 runs

the particle size because of the excessive agglomeration of the metallic phases, which made it difficult to distinguish and measure the different particles. These four samples were also studied by elemental mapping and the maps obtained are shown in Fig. S5. These images are consistent with the SEM mapping discussed previously, where Ni and W are well dispersed throughout the catalyst. In addition, in the Ni-W/CG, Ni-W/CO and Ni-W/CB samples, the overlap of both metals was observed by the orange areas due to the combination of red and yellow (Ni and W, respectively). In these catalysts, there is a very high overlap of these metals, indicating that their presence is very similar throughout the catalyst and that both active centres are close to each other. On the other hand, the Ni-W/CB after reutilization showed a higher separation of both metals, with several areas of only W and some areas where Ni predominated over W, as indicated by the redder colour of the mapped area.

The active phases present on the catalysts were analyzed by XRD and the results obtained are displayed in Fig. 6. The spectra were analyzed using the X'Pert Highscore software, which helped identify and quantify the different species (Table S1). All samples displayed peaks characteristic of Ni (ref. code 03–065-2865) at ca. 2θ = 44.5°, 51.8°, 76.4° and 92.9°, and $NiWO_4$ (ref. code 01–072-1189) at ca. 2θ = 24.0°, 25.9°, 30.9°, 36.6°, 52.4° and 54.7°. Furthermore, a WO_2 peak (ref. code 00–032-1393) at ca. 2θ = 25.8°, 31.6°, 36.8° and 52.9°, which partially overlaps the $NiWO_4$ peaks, was observed in all samples except in the catalyst after the recyclability measurements. Additionally, the fruit peel derived-carbons also presented $CaWO_4$ peaks (ref. code 01–077-2233) at ca. 2θ = 18.6°, 28.7°, 34.1°, 39.1°, 47.1°, 49.1°, 57.9° and 64.6°, due to the calcium present in the orange/banana carbon supports, which is in agreement with the EDS spectra. The high presence of the Ni phase indicates that the reduction of nickel was successful. The oxidized species of Ni (NiO and NiO_2) were not detected in the obtained XRD spectra. Considering the XPS results presented (Table 2), the Ni^{2+} species observed in that analysis correspond to the Ni present in the $NiWO_4$ detected by XRD. Therefore, the increase of Ni^{2+} observed in the XPS spectra after the reusability assessments is correlated with the rearrangement of the Ni species into $NiWO_4$ as observed in Table S1. Although the presence of Ni^0 after cycles decreases in both XPS and XRD, the increase of $NiWO_4$ balances the loss of activity by also acting as an active site towards the EG formation.

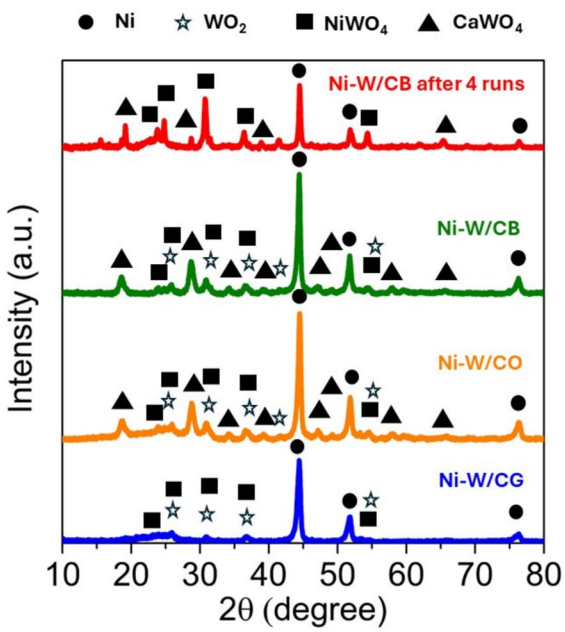

Fig. 6 XRD patterns of the Ni-W bimetallic catalysts

The Ni crystallite size (Table 1) of the different catalysts was also determined using the Scherrer equation (Kawsar et al. 2024). The lowest value (16.9 nm) was calculated for the CG sample, which may be due to its more regular shape than the fruit waste-derived carbons, which may have led to a very good distribution of the metallic species (Fig. S5) and, consequently, lower agglomeration, resulting in the lower particle size. Regarding Ni-W/CO and Ni-W/CB, a slight increase in the particle size was observed (21.8 and 21.3 nm, respectively), which may have been related to the agglomeration of the Ni particles. Lastly, after the four successive runs of the Ni-W/CB catalyst, the Ni particle size significantly increased to 29.4 nm, which may be related to the migration of the Ni from inside the porous structures to the surface of the catalyst, as it was observed by XPS, leading to a higher agglomeration of this species.

Catalytic performance

Based on preliminary studies in which the reaction parameters were optimized, the reactions were conducted at 205 ºC under 50 bar of H_2 for 5 h (Ribeiro et al. 2022, 2018a). Furthermore, an initial blank experiment, conducted without catalyst, revealed the production of only traces of polyols after 5 h, without any EG formed, despite a conversion of cellulose of 56%. Also, tests using only the CG support (without metals) still showed no EG production and a low formation of polyols due to the absence of appropriate active sites, although the conversion of cellulose increased to about 90%. These observations are consistent with those previously found by our group using CNT and glucose-derived carbon materials (Ribeiro et al. 2022, 2024; Morais et al. 2024). On the other hand, the monometallic Ni/CG catalyst (20 wt % Ni) promoted relatively high yields of polyols (e.g., 24.8% sorbitol) with a low EG yield of 10.1%. In this case, the superior hydrogenation capability of Ni favoured the production of polyols like sorbitol.

Hence, the design of a catalyst for cellulose conversion to EG in hydrothermal conditions requires a good balance of hydrogenation and RAC activities. In this sense, a Ni-W bimetallic catalyst supported on the glucose-derived carbon (Ni-W/CG) was synthesized using previously optimized metal contents (i.e., 20 wt % Ni and 10 wt % W) (Ribeiro et al. 2024). This Ni and W ratio led to the following conversion route, as previously reported: i) hydrolysis of cellulose to glucose, catalysed by the H^+ produced by high temperature water and acid sites of the catalyst; ii) glucose RAC to glycolaldehyde, favoured by tungsten species; and iii) glycolaldehyde hydrogenation to EG, favoured by Ni active sites (Morais et al. 2024; Ribeiro et al. 2024; Gao et al. 2023). Subsequently, Ni-W/CG was tested for the conversion of cellulose and the results are presented in Table 3. The total yields of identifiable products over Ni-W/CG were 71%, in which the main product was EG (50.1%), along with propylene glycol, sorbitol, threitol, erythritol, glycerol, formic acid, dihydroxyacetone and hydroxyacetone in small quantities (0.3–6.7%). This result is amongst the best EG yields reported to date, for the environmentally friendly conversion of cellulose over carbon-supported metal catalysts, as later discussed. However, a small leaching of both metals was observed in the final liquid solution recovered from the reaction (Table S2): 3.9% Ni and 7.0%W.

Then, aiming to valorize food waste for the catalyst formulation, the catalytic activity of the fruit peels-derived carbon supported catalysts was evaluated for the one-pot conversion of cellulose to EG (Table 3). Both catalysts were considerably selective for EG production. Therefore, the use of fruit peel waste herein presents a more economical option for synthesizing carbon-supported heterogeneous catalysts. Despite the small differences in the remaining identified products' distribution for the two catalysts, Ni-W/CB presented a higher yield of EG (44.3%) when compared to Ni-W/CO (34.7%), which, on the other hand, had a higher production of unidentified products (34.5 *vs.* 26.9%). Additionally, the final reaction liquid mixture was analyzed to test for metals' leaching. A small amount of nickel was detected (0.8 and 3.5% for Ni-W/CB and Ni-W/CO, respectively), while a slightly higher amount of tungsten was observed (12.6 and 13.8% for Ni-W/CB and Ni-W/CO, respectively) (Table S2). Thus, the higher performance of Ni-W/CB compared to Ni-W/CO could also relate to the higher metal leaching observed for Ni-W/CO. In addition, the better performance of the glucose-derived catalyst compared to the waste-derived ones could be related to its smaller Ni crystallite size: 16.9 nm for Ni-W/CG *vs.* 21.3–21.8 nm for the waste-derived catalysts (Table 1).

To conclude, the catalyst's reusability is a key indicator of its potential for industrial application, especially when it comes to tackling the critical challenge of determining the economic viability of EG production. The one-pot conversion of cellulose to EG occurs in compressed hot water, which requires a hydrothermal and acid leaching resistant catalyst. Thereby, the reusability of the best performing waste-derived catalyst was assessed. As shown in Table 3, a complete conversion of cellulose and 46.2% of EG yield were reached at the 4th run. Thus, Ni-W/CB showed excellent stability up to 4 cycles, without any loss of catalytic activity. The Raman results

Table 3 Catalytic results of cellulose conversion and yield of products[a]

Entry	Catalyst	X (%)	Yields[b] (%)									
			EG	PG	SOR	THR	ERY	GLY	FA	DHA	HA	Others
1	Ni-W/CG	100	50.1	3.8	6.7	1.2	1.3	2.7	1.4	0.3	3.5	29.0
2	Ni-W/CO	100	34.7	2.7	12.2	1.2	2.2	3.2	3.7	3.0	2.6	34.5
3	Ni-W/CB	100	44.3	3.8	9.5	1.0	2.1	2.9	3.6	2.7	3.2	26.9
4	Ni-W/CB (after 2nd run)	100	47.1	4.1	9.9	1.6	2.0	3.1	0.0	3.0	5.0	24.2
5	Ni-W/CB (after 3rd run)	100	45.0	4.6	8.7	1.6	1.8	3.2	1.2	2.8	4.7	26.4
6	Ni-W/CB (after 4th run)	100	46.2	3.9	7.3	1.5	1.2	3.5	0.0	0.9	9.2	26.3

[a]Reaction conditions: ball-milled cellulose (0.75 g), catalyst (0.3 g), H_2O (0.3 L), 205 ºC, 50 bar H_2, 300 rpm, 5 h

[b]*EG* ethylene glycol, *PG* propylene glycol, *SOR* sorbitol, *THR* threitol, *ERY* erythritol, *GLY* glycerol, *FA* formic acid, *DHA* dihydroxyacetone, *HA* hydroxyacetone

indicated that the A_D/A_G ratio of Ni-W/CB remained similar before and after reutilization, indicating no significant structural changes in the carbon material. On the other hand, the N_2 adsorption–desorption results of the fresh and used catalyst (Table 1) indicated that the specific surface area decreased from 358 to 239 $m^2\ g^{-1}$ after reuse, which was accompanied by a decrease of the micropores and an increase of the external surface area. Also, the reused catalyst exhibited higher concentrations of Ni on its surface than the fresh Ni-W/CB catalyst, as evidenced by XPS and EDS analyses. However, practically no metallic Ni or W was detected on the catalyst's surface following the reusability runs. Furthermore, the Ni crystallite size estimated by XRD also suffered an increase from 21.3 to 29.4 nm after the reutilization experiments (Table 1). Nonetheless, the catalyst kept hydrothermally stable in acid reaction conditions, so the yield of EG did not decrease after the four reutilization runs. Accordingly, in this work, we report the synthesis of an efficient, selective and stable food waste-derived carbon supported Ni-W catalyst for the production of EG directly from cellulose using an environmentally friendly process.

Lastly, since it directly depends on many variables (e.g., H_2 pressure, reaction temperature and time, substrate concentration and type), it is very difficult to compare the present catalytic performance to those previously reported. Nevertheless, we made an effort to place the EG yields found here within the existing literature. In that regard, some groups have devoted their work to the development of Ru-W catalysts for cellulose conversion to EG. For example, Zheng et al. (Zheng et al. 2010) and Zhang et al. (Zhang et al. 2019) accomplished remarkable EG yields around 62% from microcrystalline cellulose (MCC) using Ru-W catalysts supported on activated carbon (AC) and graphene, respectively (Table 4). However, the conditions used were very harsh (245 ºC and > 60 bar of H_2), and was accompanied by a loss of catalytic performance after repeated use. Likewise, our group also developed Ru-W catalysts: an initial study reported carbon nanotubes supported catalysts (Ribeiro et al. 2018b), while a subsequent study presented glucose-derived carbon supported catalysts (Ribeiro et al. 2019). The fact that we used ball-milled cellulose (BMC) allowed us to use less drastic reaction conditions (i.e., 205 ºC and final H_2 pressure of 50 bar) in comparison to the previously mentioned groups (Table 4), although the EG yields obtained were slightly lower (up to 48.4%). In addition, as far as we are concerned, only one group has reported so far the conversion of cellulose to EG using waste-derived catalysts. In this case, Huang et al. reported a Ru-W catalyst supported on biochar produced from pomelo peel, and managed to achieve an EG yield of 68.8% in 10 h (Table 4) (Huang et al. 2022). This EG yield was one of the highest attained to date, but a substantial decrease in the yield was observed after the fourth run: 65% relative EG yield loss. Accordingly, despite presenting a lower EG yield, the waste-derived catalyst developed herein (i.e., Ni-W/CB) is capable of working under less harsh reaction conditions (e.g., 205 ºC) and still maintain an EG yield around 45% after just 5 h in four successive runs with the same catalyst sample, thereby showing no catalyst deactivation after repeated use.

On another point of view, all the mentioned previously reported works have a common drawback: the high price of noble Ru. Therefore, considering the replacement of Ru by cheaper metals, many other works have been reporting in the past years Ni-W catalysts for this application (Table 4). For example, EG yields of 49.8, 46.0 and 51.0% were indicated from MCC over 2Ni-30W_2C/AC (Ji et al. 2008), 2Ni-20WP/AC (Zhao et al. 2010) and 9Ni-52W/NC (Boulos et al. 2024), respectively, which are similar to those obtained in the present work. Moreover, compared to other catalysts that were previously reported under the exact same operation condition, such as Ni-W/CNT (Ribeiro et al. 2022), Ni-W/AG (Ribeiro et al. 2024), Ni-W/AG-CNT (Morais et al. 2024) and Ni-W/CG (this work), not only the EG yield obtained from BMC but also the stability of Ni-W/CB is similar or even better in some cases. More recently, Goc et al. also elevated the EG yield directly produced from MCC to 60% over 5Ni-30W_2C/AC (Goc et al. 2023). However, once more, the conditions used were much harsher (245 ºC and > 60 bar of H_2) than those used herein. Finally, Gao et al. (Gao et al. 2023) and Wu et al. (Wu et al. 2024) developed Ni-W catalysts supported on glucose-based carbons, which also allowed to attain EG yields higher than 60% at 220 ºC. However, these catalysts showed some deactivation upon repeated use (Table 4). Accordingly, the results obtained here over Ni-W/CG (50.3%) and Ni-W/CB (around 45%) are amongst the best ever reported for the direct conversion of cellulose to EG

Table 4 Comparison of the synthesized catalysts with other carbon-supported catalysts reported in the literature

Entry	Substrate	Catalyst	Catalyst/Substrate (w/w)	T (° C)	P_{H_2}(bar)	t (h)	X (%)	Y_{EG} (%)	Relative Y_{EG} loss after reuse (%)	Reference
1	MCC (1 wt %)	5Ru-25W/AC	0.3	245	60 [a]	0.5	100	61.7	N.D	(Zheng et al. 2010)
2	MCC (1 wt %)	5Ru-30$W_{18}O_{40}$/graphene	0.1	245	60 [a]	1	100	62.5	22 (3 cycles)	(Zhang et al. 2019)
3	BMC (0.25 wt %)	0.4Ru-30W/CNT	0.4	205	50	3	100	42.4	3 (3 cycles)	(Ribeiro et al. 2018b)
4	BMC (0.25 wt %)	0.4Ru-30W/CG	0.4	205	50	5	100	48.4	14 (3 cycles)	(Ribeiro et al. 2019)
5	MCC (1 wt %)	5Ru-40WO_x/BC	1	220	30 [a]	10	99.8	68.8	65 (4 cycles)	(Huang et al. 2022)
6	MCC (1 wt %)	2Ni-30W_2C/AC	0.3	245	60 [a]	0.5	95	49.8	14 (3 cycles)	(Ji et al. 2008)
7	MCC (1 wt %)	2Ni-20WP/AC	0.3	245	60 [a]	0.5	100	46.0	N.D	(Zhao et al. 2010)
8	MCC (1 wt %)	5Ni-30W_2C/AC	0.3	245	60 [a]	1	-	60.0	15 (3 cycles)	(Goc et al. 2023)
9	MCC (1 wt %)	9Ni-52W/NC	0.3	245	90 (60 [a])	1	-	51.0	N.D	(Boulos et al. 2024)
10	BMC (0.25 wt %)	20Ni-20W/CNT	0.4	205	50	5	100	50.3	16 (6 cycles)	(Ribeiro et al. 2022)
11	BMC (0.25 wt %)	20Ni-10W/CNT	0.4	205	50	5	100	42.3	N.D	(Ribeiro et al. 2022)
12	MCC (0.8 wt %)	9Ni-13.5W/GC	0.5	220	50 [a]	2	100	69.2	16 (6 cycles)	(Gao et al. 2023)
13	MCC (0.8 wt %)	9Ni-12WO_x/GC	0.5	220	50 [a]	2	100	63.0	13 (6 cycles)	(Wu et al. 2024)
14	BMC (0.25 wt %)	20Ni-10W/AG	0.4	205	50	5	100	62.1	16 (4 cycles)	(Ribeiro et al. 2024)
15	BMC (0.25 wt %)	10Ni-5W/AG-CNT	0.4	205	50	5	100	61.7	9 (4 cycles)	(Morais et al. 2024)
16	BMC (0.25 wt %)	20Ni-10W/CG	0.4	205	50	5	100	50.1	N.D	This work
17	BMC (0.25 wt %)	20Ni-10W/CB	0.4	205	50	5	100	~45	0 (4 cycles)	This work

[a]Measured at room temperature

MCC microcrystalline cellulose, *BMC* ball-milled cellulose, *AC* activated carbon, *CNT* carbon nanotubes, *CG* carbonized glucose, *BC* pomelo peel biochar, *NC* N-doped porous carbon, *CNF* carbon nanofibers, *N.D.* not determined

over carbon-supported catalysts. Furthermore, the banana peel-derived catalyst displays here a promising stability under high temperature.

The design of biomass-derived carbon-based catalysts plays a key role across several applications due to their excellent performance characteristics. Besides the production of EG from cellulose, other applications could be considered, such as biomass conversion to sorbitol or other valuable chemicals. In fact, we have already reported the synthesis of biomass-derived carbon-supported Ru catalysts for sorbitol production from cellulose (Rey-Raap et al. 2019). In addition, these catalysts are highly efficient in energy storage systems such as supercapacitors (Rey-Raap et al. 2020), and are important towards oxygen reactions (Morais et al. 2019), which are critical for technologies such as fuel cells, electrolysers and metal-ion batteries. Moreover, their high surface area and tunable functionality make them excellent adsorbents for pollution control (Subba Reddy et al. 2024), aiding in environmental remediation. Furthermore, their biocompatibility also extends their applications into the field of biomedicine (Liu et al. 2024), demonstrating their importance throughout sustainable and advanced technologies.

Conclusions

Orange and banana peels obtained from food waste were utilized as carbon hosts for the synthesis of supported metal catalysts. Based on characterization, the waste-derived carbons and catalysts exhibited developed porous structures and successful incorporation of the metal species. Moreover, these catalysts displayed very similar textural properties and defect/graphitic nature to those of the glucose sample. The similarity between all samples allowed an almost identical metal content incorporation and dispersion on the material. Meanwhile, the synthesized catalysts demonstrated noteworthy activity in the conversion of cellulose (100%), resulting in an impressive EG yield of up to 50% over Ni-W/CG. Amongst the two waste-based catalysts, Ni-W/CB presented the best performance, allowing to produce 44.3% of EG in just 5 h. Furthermore, this catalyst exhibited admirable reusability, resulting in a yield of EG of 46.2% after four successive runs. Therefore, the present work displays a promising approach for the synthesis of catalysts with considerable catalytic activity in cellulose conversion to EG, thereby enhancing the high-value utilization of biomass and residues. As future work, an evaluation of the long-term catalytic performance, an economic study and scalability analysis could be carried out to better understand the feasibility and viability of our processes.

Acknowledgements This work was supported by national funds through FCT/MCTES (PIDDAC): LSRE-LCM, UIDB/50020/2020 (https://doi.org/10.54499/UIDB/50020/2020) and UIDP/50020/2020 (https://doi.org/10.54499/UIDP/50020/2020); ALiCE, LA/P/0045/2020 (https://doi.org/10.54499/LA/P/0045/2020); and project BiCat4Energy (PTDC/EQU-EQU/1707/2020). Authors are thankful to CEMUP for the assistance with SEM and to Universidade de Trás-os-Montes e Alto Douro (UTAD) for the XRD analyses.

Author contributions L.S. Ribeiro—Conceptualization, methodology, validation, investigation, data curation, writing—original draft preparation, writing—review and editing. R.G. Morais—Conceptualization, methodology, validation, investigation, data curation, writing—original draft preparation, writing—review and editing. A.C. Damas—Investigation, data curation. J.J.M. Órfão—Conceptualization, methodology, validation, writing—review and editing. M.F.R. Pereira—Conceptualization, methodology, validation, writing—review and editing, resources, funding acquisition. All authors have read and agreed to the published version of the manuscript.

Funding Open access funding provided by FCT|FCCN (b-on).

Data availability The original contributions presented in the study are included in the article/supplementary material, and any further inquiry can be directed to the corresponding author.

Declarations

Competing interests The authors declare no competing interests.

References

Boulos J, Goc F, Perret N, Rataboul F, Dhainaut J, Royer S (2024) Cellulose conversion to glycols over a carbon-supported Ni–WxC nanocatalyst: the N-doping effect on catalyst stability. ACS Appl Nano Mater 7:16086–16096. https://doi.org/10.1021/acsanm.4c01978

Ganbavle VV, Agawane GL, Moholkar AV, Kim JH, Rajpure KY (2014) Structural, optical, electrical, and dielectric properties of the spray-deposited WO_3 thin films. J Mater Eng Perform 23:1204–1213. https://doi.org/10.1007/s11665-014-0873-3

Gao M, Li Z, Zhao B, Yu S, Huang L, Wu Q (2023) Nickel-tungsten co-doped carbon-based catalyst for high selective production of ethylene glycol from cellulose hydrogenolysis. Fuel Process Technol 247:107816. https://doi.org/10.1016/j.fuproc.2023.107816

Goc F, Epicier T, Perret N, Rataboul F (2023) Preparation of carbon-supported tungsten carbides: comparative determination of surface composition and influence on cellulose transformation into glycols. ChemCatChem 15:e202201496. https://doi.org/10.1002/cctc.202201496

Huang H, Chen L, Gu C, Zhang X, Liu J, Zhang Q, Wang C, Ma L, Liao Y (2022) In-situ synthesis of Ru–WOX/biochar catalyst for conversion of cellulose toward ethylene glycol. Cellulose 29:8195–8211. https://doi.org/10.1007/s10570-022-04794-1

Inkoua S, Li C, Shao Y, Lin H, Fan M, Zhang L, Zhang S, Hu X (2023) Co-hydrothermal carbonization of fruit peel with sugars or furfural impacts structural evolution of hydrochar. Ind Crops Prod 193:116221. https://doi.org/10.1016/j.indcrop.2022.116221

Ji N, Zhang T, Zheng M, Wang A, Wang H, Wang X, Chen JG (2008) Direct catalytic conversion of cellulose into ethylene glycol using nickel-promoted tungsten carbide catalysts. Angew Chem Int Ed 47:8510–8513. https://doi.org/10.1002/anie.200803233

Kawsar M, Hossain MS, Bahadur NM, Ahmed S (2024) Synthesis of nano-crystallite hydroxyapatites in different media and a comparative study for estimation of crystallite size using Scherrer method, Halder-Wagner method size-strain plot, and Williamson-Hall model. Heliyon 10:e25347. https://doi.org/10.1016/j.heliyon.2024.e25347

Kempasiddaiah M, Sree Raj KA, Kandathil V, Dateer RB, Sasidhar BS, Yelamaggad CV, Sekhar Rout C, Patil SA (2021) Waste biomass-derived carbon-supported palladium-based catalyst for cross-coupling reactions and energy storage applications. Appl Surf Sci 570:151156. https://doi.org/10.1016/j.apsusc.2021.151156

Lam SS, Liew RK, Cheng CK, Rasit N, Ooi CK, Ma NL, Ng J, Lam WH, Chong CT, Chase HA (2018) Pyrolysis production of fruit peel biochar for potential use in treatment of palm oil mill effluent. J Environ Manage 213:400–408. https://doi.org/10.1016/j.jenvman.2018.02.092

Li Y, Liao Y, Cao X, Wang T, Ma L, Long J, Liu Q, Xua Y (2015) Advances in hexitol and ethylene glycol production by one-pot hydrolytic hydrogenation and hydrogenolysis of cellulose. Biomass Bioenerg 74:148–161. https://doi.org/10.1016/j.biombioe.2014.12.025

Li Y, Zhang Y, Li Z, Zhang H, Fu P (2024) Reaction pathways and selectivity in the chemo-catalytic conversion of cellulose and its derivatives to ethylene glycol: a review. Chin J Chem Eng 66:310–331. https://doi.org/10.1016/j.cjche.2023.09.013

Liu W-J, Jiang H, Yu H-Q (2015) Development of biochar-based functional materials: toward a sustainable platform carbon material. Chem Rev 115:12251–12285. https://doi.org/10.1021/acs.chemrev.5b00195

Liu Y, Zhang L, Cai H, Qu X, Chang J, Waterhouse GIN, Lu S (2024) Biomass-derived carbon dots with pharmacological activity for biomedicine: recent advances and future perspectives. Sci Bull 69:3127–3149. https://doi.org/10.1016/j.scib.2024.08.011

Ma R, Fakudze S, Shang Q, Wei Y, Chen J, Liu C, Han J, Chu Q (2021) Catalytic hydrothermal carbonization of pomelo peel for enhanced combustibility of coal/hydrochar blends and reduced CO_2 emission. Fuel 304:121422. https://doi.org/10.1016/j.fuel.2021.121422

Miah T, Demoro P, Nduka I, De Luca F, Abate S, Arrigo R (2023) Orange peel biomass-derived carbon supported cu electrocatalysts active in the CO_2-reduction to formic acid. ChemPhysChem 24:e202200589. https://doi.org/10.1002/cphc.202200589

Morais RG, Rey-Raap N, Figueiredo JL, Pereira MFR (2019) Glucose-derived carbon materials with tailored properties as electrocatalysts for the oxygen reduction reaction. Beilstein J Nanotechnol 10:1089–1102. https://doi.org/10.3762/bjnano.10.109

Morais RG, Ribeiro LS, Órfão JJM, Pereira MFR (2024) Low-cost Ni-W catalysts supported on glucose/carbon nanotube hybrid carbons for sustainable ethylene glycol synthesis. Molecules 29:3962. https://doi.org/10.3390/molecules29163962

Moulder JF, Chastain J (1992) Handbook of X-ray photoelectron spectroscopy: a reference book of standard spectra for identification and interpretation of XPS Data. Physical electronics division perkin-elmer corporation.

Orozco RS, Hernández PB, Morales GR, Núñez FU, Villafuerte JO, Lugo VL, Ramírez NF, Díaz CEB, Vázquez PC (2014) Characterization of lignocellulosic fruit waste as an alternative feedstock for bioethanol production. BioResources 9:1873–1885

Rey-Raap N, Ribeiro LS, Órfão JJM, Figueiredo JL, Pereira MFR (2019) Catalytic conversion of cellulose to sorbitol over Ru supported on biomass-derived carbon-based materials. Appl Catal B 256:117826. https://doi.org/10.1016/j.apcatb.2019.117826

Rey-Raap N, Granja MAC, Pereira MFR, Figueiredo JL (2020) Phosphorus-doped carbon/carbon nanotube hybrids as high-performance electrodes for supercapacitors. Electrochim Acta 354:136713. https://doi.org/10.1016/j.electacta.2020.136713

Ribeiro LS, Órfão JJM, Pereira MFR (2015) Enhanced direct production of sorbitol by cellulose ball-milling. Green Chem 17:2973–2980. https://doi.org/10.1039/C5GC00039D

Ribeiro LS, Órfão J, Órfão JJM, Pereira MFR (2018a) Hydrolytic hydrogenation of cellulose to ethylene glycol over carbon nanotubes supported Ru-W bimetallic

catalysts. Cellulose 25:2259–2272. https://doi.org/10.1007/s10570-018-1721-7

Ribeiro LS, Órfão JJM, Pereira MFR (2018b) Insights into the effect of the catalytic functions on selective production of ethylene glycol from lignocellulosic biomass over carbon supported ruthenium and tungsten catalysts. Biores Technol 263:402–409. https://doi.org/10.1016/j.biortech.2018.05.034

Ribeiro LS, Rey-Raap N, Figueiredo JL, Órfão JJM, Pereira MFR (2019) Glucose-based carbon materials as supports for the efficient catalytic transformation of cellulose directly to ethylene glycol. Cellulose 26:7337–7353. https://doi.org/10.1007/s10570-019-02583-x

Ribeiro LS, Pires ALF, Órfão JJM, Pereira MFR (2022) Paving the way towards an eco- and budget-friendly one-pot catalytic conversion of cellulose and lignocellulosic residues into ethylene glycol over Ni-W/CNT catalysts. Renew Energy 200:1008–1022. https://doi.org/10.1016/j.renene.2022.10.026

Ribeiro LS, Morais RG, Órfão JJM, Pereira MFR (2024) Unlocking the value of food waste: sustainable production of ethylene glycol over low-cost Ni-W catalysts supported on glucose-derived carbons. Sustain Energy Fuels 8:4588–4601. https://doi.org/10.1039/D4SE00823E

Satira A, Paone E, Bressi V, Iannazzo D, Marra F, Calabrò PS, Mauriello F, Espro C (2021) Hydrothermal carbonization as sustainable process for the complete upgrading of orange peel waste into value-added chemicals and biocarbon materials. Appl Sci. https://doi.org/10.3390/app112210983

Shetty A, Molahalli V, Sharma A, Hegde G (2023) Biomass-derived carbon materials in heterogeneous catalysis: a step towards sustainable future. Catalysts. https://doi.org/10.3390/catal13010020

Subba Reddy Y, Rotte NK, Sudhakar BK, Ramakrishna Chand N, Naik RJ, Mandal S, Ravi Chandra M (2024) Biomass-derived sustainable mesoporous activated carbon as an efficient and recyclable adsorbent for the adsorption of hazardous dyes. Hybrid Adv 6:100218. https://doi.org/10.1016/j.hybadv.2024.100218

Teng Y, Zhou L, Chen Y-Z, Gan J-Z, Xi Y, Jia H-L (2023) Orange-peel derived carbon-loaded low content ruthenium nanoparticles as ultra-high performance alkaline water HER electrocatalysts. Dalton Trans 52:15839–15847. https://doi.org/10.1039/D3DT02969G

Tran LT, Nguyen MQ, Hoang HT, Nguyen HT, Vu THT (2022) Catalytic hydrothermal carbonization of avocado peel. J Chem 2022:5766269. https://doi.org/10.1155/2022/5766269

Wang A, Zhang T (2013) One-pot conversion of cellulose to ethylene glycol with multifunctional tungsten-based catalysts. Acc Chem Res 46:1377–1386. https://doi.org/10.1021/ar3002156

Wang S, Cheng A, Liu F, Zhang J, Xia T, Zeng X, Fan W, Zhang Y (2023) Catalytic conversion network for lignocellulosic biomass valorization: a panoramic view. Indus Chem Mater 1:188–206. https://doi.org/10.1039/d2im00054g

Worldostats. 2024. Accessed December 4, 2024. https://worldostats.com/most-produced-fruits-in-the-world-2024/.

Wu Q, Wang Z, Zhao B, Zhao R, Yu S, Huang L (2024) Nickel-tungsten co-doped biochar catalyst boosting ethylene glycol production from cellulose hydrogenolysis. Ind Crops Prod 207:117752. https://doi.org/10.1016/j.indcrop.2023.117752

Yadav G, Ahmaruzzaman M (2022) Citrus limetta peel-derived catalyst for sustainable production of biodiesel. ACS Omega 7:28534–28544. https://doi.org/10.1021/acsomega.2c03314

Yadav R, Joshi P, Hara M, Yana T, Hashimoto S, Yoshimura M (2020) Intercorrelation between physical and electrochemical behavior of nitrogen-doping in graphene for symmetric supercapacitor electrode. SN Appl Sci 2:1630. https://doi.org/10.1007/s42452-020-03401-x

Zhang K, Yang G, Lyu G, Jia Z, Lucia LA, Chen J (2019) One-pot solvothermal synthesis of graphene nanocomposites for catalytic conversion of cellulose to ethylene glycol. ACS Sustain Chem Eng 7:11110–11117. https://doi.org/10.1021/acssuschemeng.9b00006

Zhao G, Zheng M, Wang A, Zhang T (2010) Catalytic conversion of cellulose to ethylene glycol over tungsten phosphide catalysts. Chin J Catal 31:928–932. https://doi.org/10.1016/S1872-2067(10)60104-0

Zheng MY, Wang AQ, Ji N, Pang JF, Wang XD, Zhang T (2010) Transition metal-tungsten bimetallic catalysts for the conversion of cellulose into ethylene glycol. Chemsuschem 3:63–66. https://doi.org/10.1002/cssc.200900197

Zhu Z, Yu G, Duan L, Liu X, Wang L, Zhang J (2023) Nickel phthalocyanine modified fruit-peel-derived carbon framework selectively electro-catalyzes CO_2-to-CO conversion. J Mol Liq 376:121432. https://doi.org/10.1016/j.molliq.2023.121432

Ziegler D, Palmero P, Giorcelli M, Tagliaferro A, Tulliani J-M (2017) Biochars as innovative humidity sensing materials. Chemosensors. https://doi.org/10.3390/chemosensors5040035